Resonant cavities with phase-changing materials

Article *in* Optics Letters · November 2017

DOI: 10.1364/OL.42.004784

CITATIONS
9

READS
205

3 authors:

Roney Thomas
Wesleyan University
23 PUBLICATIONS **243** CITATIONS
SEE PROFILE

Ilya Vitebskiy
Wright-Patterson Air Force Base
77 PUBLICATIONS **2,049** CITATIONS
SEE PROFILE

Tsampikos Kottos
Wesleyan University
311 PUBLICATIONS **11,314** CITATIONS
SEE PROFILE

Optics Letters

Resonant cavities with phase-changing materials

Roney Thomas,[1,*] Ilya Vitebskiy,[2] and Tsampikos Kottos[1]

[1]Department of Physics, Wesleyan University, 265 Church St., Middletown, Connecticut 06457, USA
[2]Air Force Research Laboratory, Sensors Directorate, Wright-Patterson Air Force Base, Ohio 45433, USA
*Corresponding author: rthomas03@wesleyan.edu

Received 12 September 2017; revised 21 October 2017; accepted 25 October 2017; posted 26 October 2017 (Doc. ID 306981); published 16 November 2017

Phase changing materials are commonly used for optical switching, limiting, and sensing. In many important cases, the change in the transmission characteristics of the optical material is caused by light-induced heating. We demonstrate that the incorporation of such optical materials in judiciously designed photonic structures can dramatically alter the light-induced phase change, as well as the transmission characteristics of the entire photonic structure. Possible practical implications are discussed.

OCIS codes: (160.6990) Transition-metal-doped materials; (250.6715) Switching; (310.4165) Multilayer design; (050.2770) Gratings.

https://doi.org/10.1364/OL.42.004784

There are many examples of optical materials where a nonlinear absorption increases with light intensity. This increase is attributed to different mechanisms, some of which can result in a nearly instantaneous adjustment of the absorption coefficient to the light intensity, as in the case of two-photon absorption [1,2]. In this Letter, we consider another important scenario where the increase in absorption is caused by light-induced heating [3,4]. The related problems have been addressed in numerous publications devoted to the interaction of laser radiation with optical materials [5,6]. The temperature dependence of the absorption coefficient can be gradual, or it can be abrupt. The latter example is presented by vanadium dioxide (VO_2), undergoing an isolator-to-metal phase transition when heated above $T_C = 68°C$. We refer to such types of materials as phase-change materials (PCM) [7,8].

In this Letter, we consider the case of a layer of optical material with heat-induced absorption being sandwiched between two lossless Bragg mirrors. At low light intensity, this microcavity displays a strong resonant transmission at the frequency of the localized (defect) mode. In [9–11], we demonstrated that the light-induced absorption in such systems displays a rather peculiar behavior. At first, the absorption is enhanced by the resonant cavity but, as the light intensity increases further, the resonant (defect) mode becomes suppressed, and the entire layered structure turns highly reflective—not absorptive, as would be the case with a SA layer made of the same lossy material. This effect can be attractive for optical limiting, switching and, possibly, mode locking.

The question we address here is what happens if the absorption in the defect layer is not a gradual function of temperature but, instead, it experiences an abrupt change because of the phase transition caused by the light-induced heating. This is exactly the case with the VO_2-based resonant cavity which we shall use in our numerical investigations below. It is a complicated numerical problem involving the solution of Maxwell equations coupled with heat generation and transfer equations.

We show that in the continuous-wave (CW) case, the transmittance as a function of the light intensity and the exposure time are strikingly different from the previously studied cases: (a) the case when absorption is gradually changing with temperature [11], and (b) the case of short pulses with either gradual or abrupt temperature dependence of absorption [9]. We perform a transient and steady-state analysis using a multi-scale physics approach which takes into consideration both the electromagnetic and thermal transport effects. Special attention is given to the analysis of the time duration required to turn the photonic structure from a transmissive to a reflective mode. Our findings indicate that a judiciously designed layered structure can act as a hypersensitive reflective limiter or a switch. We show that the critical irradiance and the timescale for which the photonic structure changes its transport properties can be tailored to meet specific needs associated with various applications, such as optical sensing, switching, or limiting. The numerical analysis is carried out at 4 μm, but the main conclusions qualitatively apply to any other frequency range.

We consider a multi-layered photonic structure (MLPS) which consists of quarter-wave layers of low-index (n_L) alternating with high-index (n_H) layers. For the numerical demonstration, we assume that the respective indices are $n_L = 1.3927$ and $n_H = 2.394$ which correspond to SiO_2 and Si_3N_4. The MLPS represents a bandgap structure with high transmission bands alternating with bandgaps for which the structure acts as a perfect mirror (reflector). The photonic structure incorporates a single $\lambda_0/2.5$ (≈550 nm) defect layer D made of a PCM which is placed at its mirror symmetry plane. We have also considered MLPS with multiple PCM defects placed in a way that the whole structure still respects the mirror symmetry. The geometric sequence that describes these MLPSs is $(n_L n_H)^p D[(n_H n_L)^r n_H D]^{q-1}(n_H n_L)^p$, where $p, q, r = 1, 2, 3\ldots$.

The PCM defect layer is assumed to be made of vanadium dioxide (VO_2) which experiences dielectric to metal phase transition at temperature $T_C \approx 68$°C. During this phase transition, its electrical conductivity changes by three to four orders of magnitude [12,13]. This abrupt variation can be modeled by the following temperature-dependent change of the imaginary part of the permittivity $\epsilon_D''(T)$:

$$\epsilon_D''(T) = \epsilon_0'' + \left[\frac{\Delta\epsilon_D''}{\exp[-(T - T_C)/\delta] + 1}\right]. \quad (1)$$

In Eq. (1), $\epsilon_0'' = 0.02$ and $\Delta\epsilon_D'' \approx 25$. These were obtained by extracting its experimental values from the literature [12] and fitting Eq. (1) to them. We note that the jump in ϵ_D'' depends on a number of factors, including the preparation and quality of the VO_2 material, as well as the experimental procedures used to evaluate its complex permittivity. In fact, the real part of the permittivity ϵ_D' also changes with temperature but, since the variation is small, we shall disregard it below. Finally, δ provides a "smoothing" of the phase transition and is assumed to be $\delta = 4$°C.

During the phase transition, the VO_2 layer(s) release a latent heat which leads to a singular temperature dependence of the specific heat capacity at constant pressure C_p^D. Measurements indicated that these changes of C_p^D can be described by $C_p^D(T) = C_p^{(0)} + \frac{H_L}{\Delta\sigma_t}\frac{d\sigma}{dT}$, where the second term on the right-hand side describes the excess latent heat released by the layer due to the phase transition. We have assumed that $H_L \approx 5.042 \cdot 10^4$ J/kg [14], and $C_p^{(0)} \approx 700$ Jkg^{-1} K^{-1}. Finally, $\Delta\sigma_t \sim 9.96 \cdot 10^4$ (S/m) is the total conductivity jump during the phase transition consistent with $\epsilon_D''(T)$ of Eq. (1). Furthermore, we have taken into consideration that the thermal conductivity k_D of the PCM defect layer changes from $k_D = 4\frac{W}{mK}$ in the dielectric phase to $k_D = 6\frac{W}{mK}$ in the metallic phase.

The wave propagation along the z-direction is described by

$$\vec{\nabla} \times \vec{H} = \vec{j}_0 + \epsilon(z)\frac{\partial \vec{E}}{\partial t}, \qquad \vec{\nabla} \times \vec{E} = -\mu_0 \frac{\partial \vec{H}}{\partial t}, \quad (2)$$

where $\epsilon(z) = \epsilon'(z) + i\epsilon''(z)$ is the layers permittivity, and $\vec{j}_0 = \sigma_0(z)\vec{E}$ is the electric current. The quantity $\epsilon''(z)$ determines the losses not associated with electric conductivity.

Equation (2) is solved, together with the heat-transfer equation

$$\rho_D C_p^D \frac{\partial T}{\partial t} - \vec{\nabla} \cdot (k_D \vec{\nabla} T) = Q + q_0 + q_r, \quad (3)$$

where ρ_D is the mass density of the defect PCM layer, Q is the heat production per unit volume of the PCM layer, $q_0 = h \cdot (T_{\text{ext}} - T)$, $h = 100$ W/m^2 K is the heat flux coefficient, $T_{\text{ext}} = 20$°C denotes the temperature of the surrounding air domain, and $q_r = \epsilon_r \cdot \sigma_r \cdot (T_{\text{ext}}^4 - T^4)$ is the thermal radiation from the structure boundaries. The emissivity coefficient of SiO_2, which typically is equal to the frequency-dependent absorbance [15], is assumed for simplicity to be constant $\epsilon_r = 0.79$, and $\sigma_r = 56.7n$ W $\cdot$ m^{-2} $\cdot$ K^{-4} denotes the Stefan-Boltzmann constant. Q involves two contributions, i.e., $Q = \frac{1}{2}(\text{Real}(\vec{j}_0 \cdot \vec{E}) + \omega\epsilon''(z)\text{Real}(\vec{E} \cdot \vec{E})$. For computational convenience, we recast the above expression as $Q = \frac{1}{2}\text{Real}(\vec{j} \cdot \vec{E})$, where $\vec{j} = \sigma\vec{E}$, and $\sigma = \sigma_0 + \omega\epsilon''$. In the metallic phase, the ohmic losses associated with $\vec{j}_0 = \sigma_0(z)\vec{E}$ provide the main contribution to the heat production.

Figure 1 displays the temporal evolutions of $\mathcal{T}(t)$, $\mathcal{R}(t)$, and $\mathcal{A}(t) = 1 - \mathcal{T}(t) - \mathcal{R}(t)$ of the MLPS with $p = 5$ and $q = 1$. Two representative cases of the incident CW signal with weak (open black circles/lines) and strong (open red circles/lines) irradiance $\mathcal{I}$ are depicted. For comparison purposes, we also show $\mathcal{T}(t)$, $\mathcal{R}(t)$, and $\mathcal{A}(t)$ for a standalone (SA) VO_2 layer (filled black and red symbols and lines) whose thicknesses are kept the same as those for the MLPS case. For incident CW signals with small irradiances $\mathcal{I} = 13.3$ μW $\cdot$ cm^{-2}, $\mathcal{T}(t)$, $\mathcal{R}(t)$, and $\mathcal{A}(t)$ essentially remain constant: the transmittances in both cases acquire relatively high values for all times at frequency $\nu = 79.1$ THz with full width at half-maximum spectral width evaluated to be ≈0.41 THz; the reflectances are relatively small $\mathcal{O}(1\%)$, while the absorbance is $\mathcal{O}(1\%)$ for the SA layer and a bit higher $\mathcal{O}(10\%)$ for the case of MLPS. Nevertheless, $\mathcal{A} \sim 10\%$ does not constitute any threat (i.e., self-destruction due to overheating) for the MLPS.

In the opposite case of a high-irradiance incident CW, the transmittance of the MLPS drops abruptly to very small steady-state values of $\mathcal{T}_\infty \equiv \lim_{t\to\infty}\mathcal{T}(t)$. Comparing this value with the SA PCM-layered structure indicates that $\mathcal{T}_\infty$ is at least two orders of magnitude smaller for the MLPS. An abrupt drop in transmittance is an essential requirement of mid-infrared wave limiters whose function is to provide protection to sensitive sensors from harmful high irradiance input CW signals. It is important that this low value of $\mathcal{T}_\infty$ be smaller than the destruction value of the sensor. It must also be reached at very early times τ in

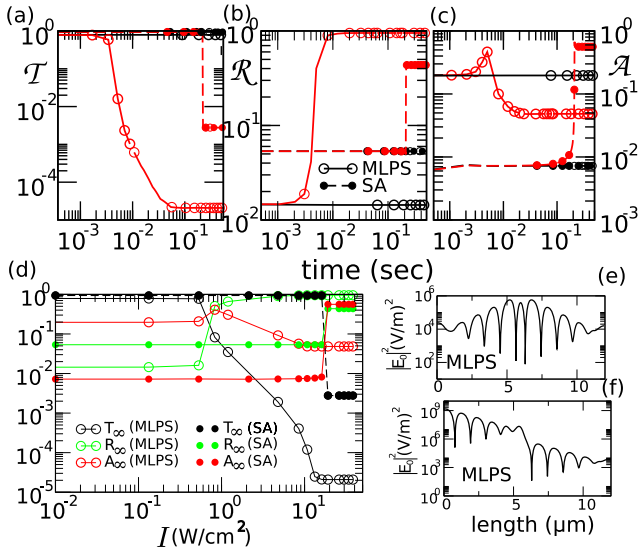

Fig. 1. (a)–(c) Typical temporal behaviors of $\mathcal{T}$, $\mathcal{R}$, and $\mathcal{A}$ for an MLPS with $p = 5, q = 1$ (open circles) and for an SA PCM layer (filled circles) of the same thickness as of the PCM defect. The SA is embedded inside a SiO_2 matrix of the same thickness as the MLPS. The black lines/circles indicate low irradiance $\mathcal{I} = 13.3$ μW $\cdot$ cm^{-2}, and the red lines/circles indicate high irradiance $\mathcal{I} = 26.03$ W·cm^{-2}. Increasing the number of bilayers leads to faster response (limiting) times (see the inset of Fig. 3). (d) Steady-state values $\mathcal{T}_\infty$, $\mathcal{R}_\infty$, and $\mathcal{A}_\infty$ versus irradiance $\mathcal{I}$ of the incident CW. The scattering electric field intensity spatial profile within the MLPS for the cases for CW signal with (e) low irradiance $\mathcal{I} = 13.3$ μW $\cdot$ cm^{-2} and (f) high irradiance $\mathcal{I} = 26.03$ W·cm^{-2}.

order to prevent destruction of the sensor due to the accumulation of energy. In our calculations, τ is defined as the activation time required by the SA or MLPS with embedded defect(s) when their respective transmittance values drop below 5%. We find that τ is smaller by at least an order magnitude for the case of MLPS, as compared to the corresponding time for the SA VO_2-layered structure. Simultaneously, we find that at τ, the reflectivity of the MLPS increases, reaching unity steady-state values $\mathcal{R}_\infty \equiv \lim_{t\to\infty} \mathcal{R}(t) \approx 1$. Finally, the steady-state absorbance $\mathcal{A}_\infty \equiv \lim_{t\to\infty} \mathcal{A}(t)$ of the MLPS decreases to values $\mathcal{O}(4\%)$–as opposed to the SA PCM layer which gets values as high as 55%. The latter represents a *self-destructive limiter* which provides protection to a sensor at the cost of its own destruction due to heating. Instead, the MLPS with PCM defect layer(s) acts as a *reflective limiter* (not absorbing!) protecting both sensitive sensors and itself from self-destruction by reflecting high irradiance incident CW signals back in space.

The abrupt drop of $\mathcal{T}_\infty$ and the transition to an (almost) complete reflective mode in the case of MLPS can be further appreciated in Fig. 1(d), where we report an overview of $\mathcal{T}_\infty$, $\mathcal{R}_\infty$, $\mathcal{A}_\infty$ versus irradiances $\mathcal{I}$ of the incident CW. These results were obtained via frequency-stationary coupled heat-transfer simulations in the limit $t \to \infty$. In Refs. [9,16], we have demonstrated the "reflective" mechanism in the case of non-linear lossy defect layers embedded in a multi-layered photonic crystal structure. However, this is activated at a cost of orders of magnitude change in the incident light intensity. In contrast, our current findings for MLPS with PCM defect layers indicate that the abrupt transition from high transmittivity to high reflectivity can occur for low incident irradiances.

Let us analyze the transition from a high transmittance to an (almost) complete reflectance in MLPS. Figures 1(e) and 1(f) display the scattering electric field intensity profile inside the MLPS, at the resonant defect frequency at low $\mathcal{I} \approx 13.3\ \mu\text{W} \cdot \text{cm}^{-2}$ (corresponding to high transmittance) and high $\mathcal{I} \approx 26.03\ \text{W} \cdot \text{cm}^{-2}$ (corresponding to high reflectance) irradiances, respectively. In the former case, the incident CW couples with the high-Q resonant defect mode of the MLPS, resulting in a high transmittivity of the incident CW. The defect mode is exponentially localized around the VO_2 layer, i.e., $|E(z)|^2 \sim \exp(-2|z - z_0|/\xi)$. ($z_0$ is the position of the defect.) The parameter ξ is the so-called localization length which depends on the permittivities, number of layers within the MLPS, and their respective widths.

The shape of the defect mode simultaneously guarantees two things. (1) The radiative losses (from the MLPS edges) are exponentially small. Thus, the resonant mode has a high-Q factor and, consequently, high transmittance. (2) The anti-nodal point of the mode coexists with the position of the PCM layer. This ensures that the critical irradiance of the incident CW, which leads to a phase change, can be exponentially small. The second feature is associated with the fact that the PCM inside the MLPS lies adjacent to a Si_3N_4 bi-layer which has a higher refractive index than that of the alternate silica layers. As a consequence, the resonant field distribution of the localized mode has a maximum (antinode) in the middle of the VO_2 defect layer. In contrast, if the defect layer were surrounded by silica layers, the resonant field distribution would have developed a nodal point at the location of the VO_2 layer.

For as long as VO_2 remains in the dielectric phase, the above two cases would behave similarly but, in the metallic regime, the two cases would differ dramatically. Indeed, if the location of the VO_2 nanolayer coincides with the maximum of the resonant field distribution, the electric conductivity of the metallic phase will immediately result in strong suppression of transmittance both inside and outside the photonic bandgap. In contrast, if the defect bi-layer was made of SiO_2, the presence of the PCM layer at the nodal point of the resonant field distribution would not affect its resonant transmittance.

The suppression of transmittance [see Fig. 1(d)] is a result of two competing dissipation mechanisms that aim to spoil the Q-factor of the mode. (a) The radiation losses via the edges of the sample are exponentially small when the VO_2 is in the dielectric phase, thus providing a high-Q factor to the mode. (b) The bulk ohmic losses associated with the PCM-filled VO_2 layer can vary and depend on the imaginary part of its complex permittivity ϵ_D. For a high enough incident radiation, when ϵ_D'' increases due to heating, the ohmic losses exceed the radiative losses. Consequently the resonant mode is completely spoiled leading to a high impedance mismatch with the incident CW signal, which results in increased reflection of the incident wave. The exponential form of the defect mode amplifies the incident irradiance and can induce an insulator-to-metal transition of the PCM at small $\mathcal{I}$.

These features are further amplified in the case of multiple q PCM defect layers; see Fig. 2. In this case, there are q resonant localized mode(s) which create a *high transmittivity mini-band for low irradiances* at the center of the bandgap; see the inset of Fig. 2(d). The electric field intensity profile is characterized by a multi-hump shape with peaks located at the position of the individual defect [blue dashed lines in Fig. 2(e)]. As in the case of one defect, when the irradiance of the incident light is above some critical value, the resonant electric field profile associated

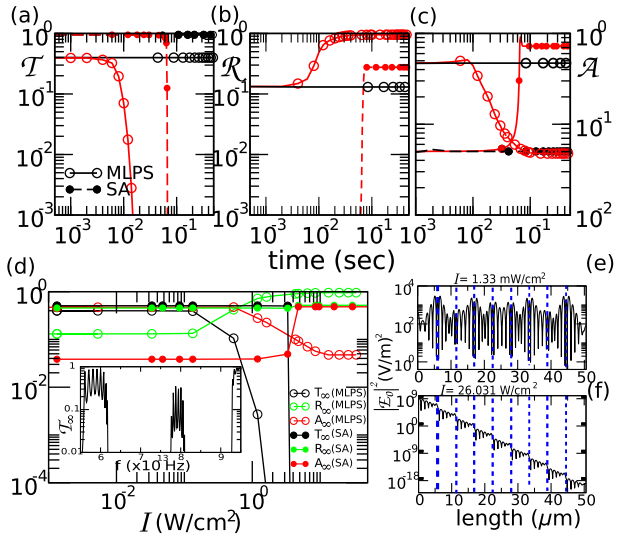

Fig. 2. Same as in Fig. 1, except for MLPS with $p = 5$, $q = 8$, and $r = 4$. The transient simulations were performed at the resonant frequency of the defect mode, $\nu = 78.96$ THz. In the inset of (d), we report the low irradiance transmission spectrum of the multi-defect case. A high transmittance mini-band at the middle of the bandgap is observed. The spatial electric field intensity profile at $\nu = 78.96$ THz for the multi-defect MLPS for input CW signal with (e) low $\mathcal{I} = 1.33\ \text{mW/cm}^2$ and (f) high $\mathcal{I} = 26\ \text{W/cm}^2$ irradiances. The blue lines indicate the position of the defects.

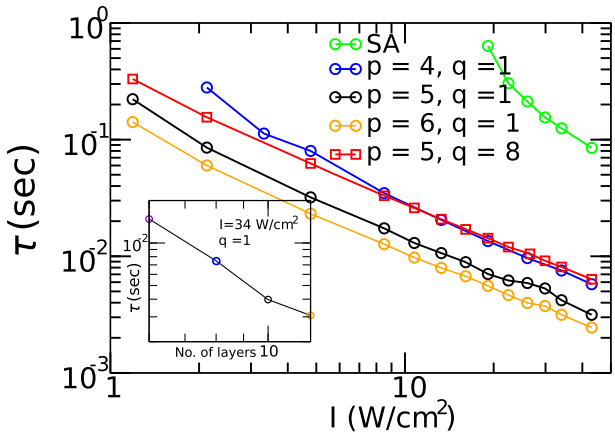

Fig. 3. Behavior of τ versus $\mathcal{I}$, for different numbers of bilayers p, and $q = 1$ (single-defect). A comparison with a MLPS ($p = 5$) with $q = 8$ and with an SA structure is shown. The inset shows τ with increasing p for a single-defect MLPS.

with the defect mode is suppressed [see Fig. 2(f)], making the structure completely reflective (not absorptive).

Let us now discuss the behavior of the "activation" time τ. We focus on the case of one defect, but the arguments apply equally well for an MLPS with multiple PCM defects.

The dependence of τ on $\mathcal{I}$ and L (where L is the total thickness of the MLPS) can be understood by considering the transport from a single PCM layer with exponentially enhanced field intensity (due to the presence of MLPS) $W \to W_{\mathrm{PCM}} \simeq W_0 \exp(L/\xi)$. ($W_0$ is the incident field intensity at the edge of the MLPS.) We further assume that the PCM layer is thin enough so that the thermal conduction through the layer is not an issue. Instead, we assume that at all times the temperature T is uniform within the PCM layer, but different from the ambient temperature T_{ext}. In the case of an embedded PCM defect, we further assume negligible thermal radiation. Taking all these considerations into account, we rewrite Eq. (3) as

$$C(T)\frac{d}{dt}T(t) = A(T)W(t) + h(T_{\mathrm{ext}} - T), \qquad (4)$$

where $C = \rho_D C_p^D$ and $A = A(T)$ is the absorbance from the PCM layer at temperature T. We further assume that the absorbance $A(T)$ experiences discontinuity at $T = T_C$, i.e., $A(T < T_C) = A_0$ and $A(T > T_C) = A_1$. Next, we consider the heating process of the PCM layer when $T < T_C$ due to an incident CW with $W(t) = W_{\mathrm{PCM}}$. In this case, ($T_{\mathrm{ext}} \le T < T_C$) the solution of Eq. (4), with initial condition $T(t = 0) = T_{\mathrm{ext}}$, is

$$T(t) = T_{\mathrm{ext}} + \frac{A_0 W_{\mathrm{PCM}}}{h}\left(1 - \exp\left(-\frac{h}{C}t\right)\right). \qquad (5)$$

The corresponding steady-state temperature is $T_\infty = T_{\mathrm{ext}} + A_0 W_0 \exp(L/\xi)/h < T_C$. The latter inequality is violated whenever the incident power is $W > W_C = (h/A_0)(T_C - T_{\mathrm{ext}})\exp(-L/\xi)$. Therefore, we conclude that the phase transition, in the case of MLPS, requires exponentially smaller incident field irradiances. The above relation explains the (exponentially) low incident irradiance threshold above which the steady-state transmittance from the MLPS decays abruptly [see Figs. 1 and 2].

Finally, an expansion of Eq. (5) for short times leads to $T(t) = T_{\mathrm{ext}} + \frac{A_0 h W_{\mathrm{PCM}}}{C} t < T_C$ which applies for as long as $t < \tau = \frac{C}{A_0 h W_{\mathrm{PCM}}}(T_C - T_{\mathrm{ext}}) \sim 1 W_0 \exp(-L/\xi)$. Eventually, at $t \ge \tau$, the PCM layer reaches the critical temperature T_C, thus triggering the phase transition. These predictions are confirmed in Fig. 3 where the activation time τ is extracted from the temporal dynamics of transmittance $\mathcal{T}(t)$ as the time at which it has dropped by 95% of its initial value, i.e., $\mathcal{T}(\tau) = 0.05\mathcal{T}(0)$.

In conclusion, using a numerical example of VO_2-based resonant cavity, we demonstrated that optical properties of a PCM can be dramatically enhanced and/or qualitatively modified by incorporating it in a judiciously designed photonic structure. This Letter study opens new opportunities for PCM applications in optical switching, limiting, and sensing, and can be tested using CW quantum cascade laser sources with powers up to ≈3 mW and a beam cross section (achieved via optical elements) $\approx 10^{-2}$ mm^2.

Funding. Office of Naval Research (ONR) (N00014-16-1-2803); National Science Foundation (NSF) (EFMA-1641109); Air Force Office of Scientific Research (AFOSR) (FA9550-14RY14COR).

Acknowledgment. The authors acknowledge partial support from ONR and NSF (R. T. and T. K.), and AFOSR (I. V.). We thank M. Kats and R. Sher for suggestions on the experimental testing of this Letter.

REFERENCES

1. E. W. V. Stryland, H. Vanherzeele, M. A. Woodall, M. J. Soileau, A. L. Smirl, S. Gupta, and T. F. Boggess, Opt. Eng. **24**, 613 (1985).
2. T. F. Boggess, S. C. Moss, I. W. Boyd, and A. L. Smirl, Opt. Lett. **9**, 291 (1984).
3. G. J. Salamo, G. C. Duree, M. Morin, E. J. Sharp, G. L. Wood, and R. R. Neurgaonkar, MRS Proc. **374**, 137 (1994).
4. M. M. Qazilbash, M. Brehm, B. G. Chae, P. C. Ho, G. O. Andreev, B. J. Kim, S. J. Yun, A. V. Balatsky, M. B. Maple, F. Keilmann, H. T. Kim, and D. N. Basov, Science **318**, 1750 (2007).
5. M. Centini, V. Roppo, E. Fazio, F. Pettazzi, C. Sibilia, J. W. Haus, J. V. Foreman, N. Akozbek, M. J. Bloemer, and M. Scalora, Phys. Rev. Lett. **101**, 113905 (2008).
6. X. Liu, J. W. Haus, and M. S. Shahriar, Opt. Express **17**, 2696 (2009).
7. M. A. Kats, D. Sharma, J. Lin, P. Genevet, R. Blanchard, Z. Yang, M. M. Qazilbash, D. N. Basov, S. Ramanathan, and F. Capasso, Appl. Phys. Lett. **101**, 221101 (2012).
8. M. A. Kats, R. Blanchard, P. Genevet, Z. Yang, M. M. Qazilbash, D. N. Basov, S. Ramanathan, and F. Capasso, Opt. Lett. **38**, 368 (2013).
9. R. Thomas, F. M. Ellis, I. Vitebskiy, and T. Kottos, "Self-regulated transport in photonic crystals with phase-changing defects," arXiv:1702.00811 (2017).
10. E. Makri, H. Ramezani, T. Kottos, and I. Vitebskiy, Phys. Rev. A **89**, 031802 (2014).
11. E. Makri, T. Kottos, and I. Vitebskiy, Phys. Rev. A **91**, 043838 (2015).
12. M. J. Dicken, K. Aydin, I. M. Pryce, L. A. Sweatlock, E. M. Boyd, S. Walavalkar, J. Ma, and H. A. Atwater, Opt. Express **17**, 18330 (2009).
13. H. W. Verleur, A. S. Barker, and C. N. Berglund, Phys. Rev. **172**, 788 (1968).
14. C. N. Berglund and H. J. Guggenheim, Phys. Rev. **185**, 1022 (1969).
15. G. Leahu, R. Li Voti, C. Sibilia, and M. Bertolotti, Appl. Phys. Lett. **103**, 231114 (2013).
16. J. H. Vella, J. H. Goldsmith, A. T. Browning, N. I. Limberopoulos, I. Vitebskiy, E. Makri, and T. Kottos, Phys. Rev. Appl. **5**, 064010 (2016).